International Communications in Heat and Mass Transfer 142 (2023) 106675

Contents lists available at ScienceDirect

International Communications in Heat and Mass Transfer

journal homepage: www.elsevier.com/locate/ichmt

Thermodynamic optimization and performance study of supercritical CO_2 thermodynamic power cycles with dry cooling using response surface method

Muhammad Ahmed [a], Abubakr Ayub [b], Nadeem Ahmed Sheikh [c,*], Muhammad Wakil Shahzad [d,*], Muhammad Haroon [a,c], Muhammad Imran [e]

[a] Department of Mechanical Engineering, Capital University of Science and Technology (C.U.S.T), Islamabad, Pakistan
[b] Department of Mechanical and Industrial Engineering (DRIMI), Universita degli Studi di Brescia, Brescia, Italy
[c] Department of Mechanical Engineering, Faculty of Engineering & Technology, International Islamic University, Islamabad, Pakistan
[d] Department of Mechanical and Construction Engineering, Northumbria University, Newcastle upon Tyne NE1 8ST, United Kingdom
[e] Department of Mechanical, Biomedical and Design Engineering, Aston University, Birmingham B4 7ET, UK

ARTICLE INFO

Keywords:
Recompression cycle
Partial cooling cycle
Supercritical carbon dioxide
ANOVA technique
Response surface method

ABSTRACT

This paper deals with thermodynamic optimization of supercritical CO_2 recompression and partial cooling cycles operating at cycle maximum temperature of 680°*C* and maximum pressure of 250 bar. The primary goal to investigate the effects of variation in heat sink temperature (ambient air temperature), mass split fraction (X), and cycle minimum pressure (P_{min}) on the thermal efficiency of the power cycles. Response surface method (RSM) is adopted to create a second-order polynomial equation in order to develop the relationship between cycle thermal efficiency and selected decision variables and to find global optimum cycle efficiency. In addition, classification of most influencing cycle parameter is carried out using ANOVA approach. In the case of a recompression cycle, the results demonstrate that heat sink temperature has the greatest impact on thermal efficiency, owing to low *p*-value and high F-value, followed by mass split fraction and minimum pressure. In a partial cooling cycle, the minimum pressure has the most significant impact on cycle thermal efficiency, followed by the mass split fraction and heat sink temperature. The global optimum combination for the recompression cycle is at heat sink temperature of 20°C, the mass split fraction of 0.3182, and a minimum pressure of 89 bar to obtain the highest thermal efficiency of 0.4963. In addition, the global optimum combination for partial cooling cycle is at heat sink temperature of 32.8 °C, mass split fraction of 0.34, and minimum pressure of 76 bar, which results in an optimum thermal efficiency of 0.4708.

1. Introduction

One of the most important aspects of industrial, economic, and political development is energy. Global energy demand will rise by 50% between 2020and 2050, according to the IEA's International Energy Outlook 2021 [1]. This would result in a 24.7% increase in annual CO_2 emissions from this sector. The engineering community has been challenged to develop renewable energy systems and enhance energy conversion efficiency to reduce the impact of climate change due to a rise in global electrical energy consumption and environmental concerns. For the majority of electric power generation, energy conversion cycles are normally coupled to a high-grade heat source like coal fired boiler, nuclear reactors and concentrated solar power tower.

The sCO_2 technology, or supercritical carbon dioxide, is among the several thermal power generation ideas proposed by researchers in the effort to improve thermodynamic cycle efficiency and reduce the carbon emissions in the power sector. The concept has received a lot of attention in recent years because of its high thermal efficiency, compact turbomachinery, eco-friendly characteristics, and ability to substitute the traditional steam Rankine cycles [2,3]. This technology can potentially make power plants more cost-effective, with lower capital expenditure and levelized cost of electricity, due to its improved thermal efficiency and compact turbomachinery [4].

In the past years, numerous efforts are carried out to analyze the

* Corresponding authors.
E-mail addresses: nadeemahmed@iiu.edu.pk (N.A. Sheikh), muhammad.w.shahzad@northumbria.ac.uk (M.W. Shahzad).

https://doi.org/10.1016/j.icheatmasstransfer.2023.106675

Available online 17 February 2023

thermodynamic and economic performance of sCO_2 cycles for applications in waste heat recovery [5–7], concentrated solar power [8,9] and other fossil fuels-based heat sources [10] with the aim to determine suitable cycle configuration. In this context, Crespi et al. [11] analyzed 38 combined and 42 stand-alone cycle configurations based on various fuels and applications. According to the data, the thermal efficiency of a basic stand-alone cycle is in the range of 40%, whereas combined cycle configurations showed efficiencies in the range of 50 to 60%. The system setups and operation characteristics of different CO_2 power cycles are reviewed by Wang et al. [12], according to the findings, the recompression cycle configuration is recommended for high-temperature heat source due to its relatively simple construction and high efficiency. Li and Eri [13] compared four sCO_2 power cycle configurations (recompression, reheated, partial cooling, and reheated partial cooling cycle) and suggested reheated partial cooling cycle as the most efficient configuration from thermodynamic point of view. T. Neises and Turchi [14] compared the performances of three supercritical CO_2 cycles (simple, recompression, and partial cooling cycles) for CSP power plants. According to the study, the partial cooling cycle demonstrated greater temperature difference across the primary heat exchanger, effectively lowering heat exchanger costs and enhancing CSP receiver efficiency.

Thermodynamic analysis of sCO_2 cycles as performed in various studies suggested compressor inlet conditions close to the critical point of CO_2 in order to benefit from lower compression work consumption due to lower compressibility factor near the critical point. However, a cooling medium temperature of 15 to 20 °C is required to achieve the compressor inlet temperature close to the critical point, which becomes difficult in hot and arid areas where cold cooling medium such as water is scarce and available air for dry cooling is typically above 30 °C [15]. This situation is common in CSP integrated sCO_2 power plants where the ambient temperature ranges usually in dry climatic conditions is between 35and 45 °C, resulting in higher compressor inlet temperatures and a significant drop in cycle efficiency [16]. In lieu of this discussion, it is important to evaluate the effect of variation in ambient temperatures on different cycle configurations as it allows to vary and optimize the cycle configuration which are less sensitive to variation in ambient temperature. In this regard, a recent work [17] provides a conceptual design of modified recompression cycle layout which is less sensitive to increase in compressor inlet temperature compared to sCO_2 recompression cycle. Khatoon et al. [18] studied the effect of varying compressor inlet temperature on thermodynamic performance of six different cycle configurations of sCO_2 cycles and CO_2-benzene mixture power cycles for dry cooled-CSP power plant. The study decided precompression cycle configuration operating with CO_2-benzene mixture as efficient layout since it showed superior cycle efficiency and larger temperature difference across primary heat exchanger.

However, in case of scarcity of naturally flowing/surface water especially in arid sites of CSP plant, alternative requirement for heat rejection is to use dry coolers in replacement of wet cooling [19]. A recent comparison found that sCO_2 cycles can maintain higher cycle efficiency when dry cooling is adopted compared to steam Rankine power cycle technology. Moreover, dry cooling is also preferable because it does not involve corrosion issue as deposition of scaling can happen in wet cooling system [20]. Thus, wet cooling may additionally require water treatment before utilizing in heat rejection.

Another important parameter in sCO_2 cycles is the split mass fraction which determines the work consumption of recompressor and temperature differences in recuperator. In [21], effect of variation in split mass fraction on cycle efficiency of sCO_2 recompression cycle is investigated. The results from the study showed that there exists an optimal value of split mass fraction at which cycle efficiency is the maximum corresponding to each turbine inlet temperature. Regarding the impact of recuperator, the work of Alawadhi et al. [22] showed that the 2% variation in effectiveness of recuperator results in 3% change in cycle efficiency of the recompression sCO_2 cycle.

According to the extensive literature review, the optimal operating conditions of the sCO_2 based cycle have been widely studied, and several research works have also documented the optimized cycle conditions and layouts for different types of heat sources. However, when it comes to the sensitivity of the sCO_2 cycle in terms of working in varying climate conditions, the thermal configuration or setting of the particular cycle remains an unanswered question especially with dry cooling. In order to continuously enhance cycle efficiency, it is necessary to establish and recommend an optimum range(s) and relationship(s) of key operation parameters for sCO_2 cycles operating in different ambient temperatures. This work provides a foundation for power block operation in the scenario of changing ambient conditions especially during heat waves and drought conditions, allowing for year-round optimal performance.

Many a times during optimization studies as well as experimental setups, one or more process variables typically depend on or be dependent upon other variables. Finding the output-vs-input relationship requires a thorough understanding of the interactions between these various variables. Likewise, design of sCO_2 thermo-power generation block relies on several factors including cycle layout parameters, design specifications and variable heat source and heat sink (ambient) conditions. Response surface method (RSM) is a statistical methodology that takes less time and is more accurate while performing optimization studies. Using a mechanism of variations in the desired variables, a response outcome is generated. One of its most important advantages is that it provides response surface of the desired response relating it to changing input parameters, which helps in examining the impact of more than one input parameters and identifying the optimum range. Multiple previous studies have looked into the potential application of RSM in optimization studies. With regards to use of RSM in power generation applications, Saeed and Kim [21] employed RSM to optimize turbine design under variable input conditions, while Goyal et al. [23] used RSM to determine the range of input parameters for maximum thermal output of ORC. RSM is also used to optimize CO_2 capture and storage technology [24], soil nailing geometric parameters [25], CNC turning process parameters [26], diffuser shape [27], air foil design [28], and in many other research fields.

In lieu of the challenges discussed earlier, this study adopted the response surface method (RSM) to:

a) Classify the key cycle parameters based on their significance towards cycle thermal efficiency,
b) Obtain optimum value of cycle parameters for the two cycle layouts
c) Provide framework for selection of cycle configuration suitable for operation in high ambient temperature.

2. System configurations

In this section, two cycle configurations considered in this paper are described.

2.1. Supercritical CO_2 recompression cycle

The layout setup of sCO_2 recompression cycle is given in Fig. 1. This setup has two compressors (the main compressor and a recompression compressor), two recuperators (high temperature and low temperature), one dry-cooler, one main heat exchanger (MHE) integrated with high temperature heat source (like CSP tower), and other components including splitter and a mixer. This layout is considered as state-of-the-art cycle layout for sCO_2 cycles in CSP and nuclear application. In this layout, CO_2 is heated in MHE (6–7), and it flows directly from the MHE at 680°C into a gas turbine to produce power (7–8). The hot stream from the turbine then passed through the HTR (8–9) to heat the high-pressure fluid going towards MHE. Then, it passed through the LTR (9–10) to heat the high-pressure fluid from the main compressor. Before dry cooler, total mass flow is split according to given split mass fraction (X) to mass splitter. The purpose of mass splitting is to balance the heat capacities in

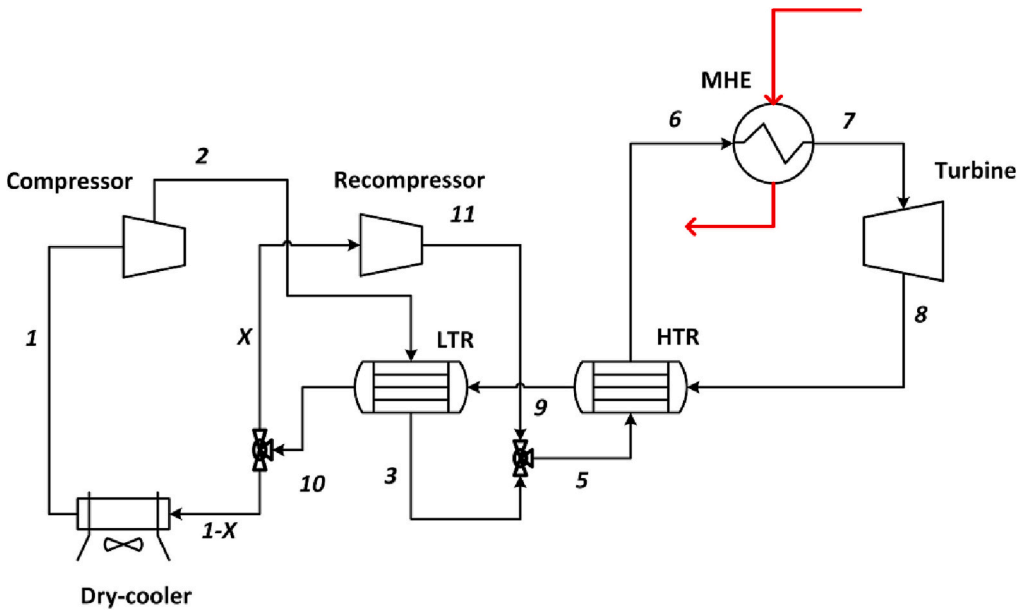

Fig. 1. Layout diagram of sCO_2 recompression cycle.

hot and cold side of LTR which enhances heat recuperation. According to the value of mass split fraction, some of the mass flow through dry cooler and main compressor before entering low temperature recuperator. Other mass of mass flow fraction after mass split is recompressed to cycle maximum pressure and mixed with high pressure stream from the LTR in the mixer. The total mass flow after mixer is finally heated in HTR and MHE to achieve cycle maximum temperature.

2.2. Supercritical CO_2 partial cooling cycle

Adding a multistage compressor with an intercooler to the recompression cycle is another way to make the power cycle more efficient. Fig. 2 shows the layout of sCO_2 partial cooling cycle. In addition to recompression cycle, this layout consists of one precooler and one precompressor. In this setup, CO_2 is heated to cycle maximum temperature (i.e. 680 $^{\circ}C$), expanded in the turbine. Then, it is cooled even more by the precooler after it passed through the HTR and LTR. The fluid is then compressed in precompressor to achieve state 12, the total mass flow is then split according to given mass split fraction. Some of the mass flow goes to the recompressor, while the rest goes towards intercooler to get to state 1 and the main compressor to get to state 2. Due to the precompression process, the pressure ratio of the recompressor is only a small part of pressure ratio of the turbine. Finally flow from the recompressor and main compressor side at cycle maximum pressure is mixed in a mixer to get total mass flow which is introduced in HTR and MHE and the cycle repeats.

2.3. Thermodynamic model

Thermodynamic properties of pure CO_2 as working fluid are computed using LK-PLOCK EoS. In a recent work by Bertini et al. [29], LK-PLOCK EoS is recommended as the most reliable and accurate model to compute VLE properties, density and specific heat of pure CO_2 as well as CO_2 + refrigerants mixtures compared to usually adopted cubic EoS.

2.3.1. Assumptions and input conditions

To develop thermodynamic models of components of sCO_2 cycle, the following assumptions are considered:

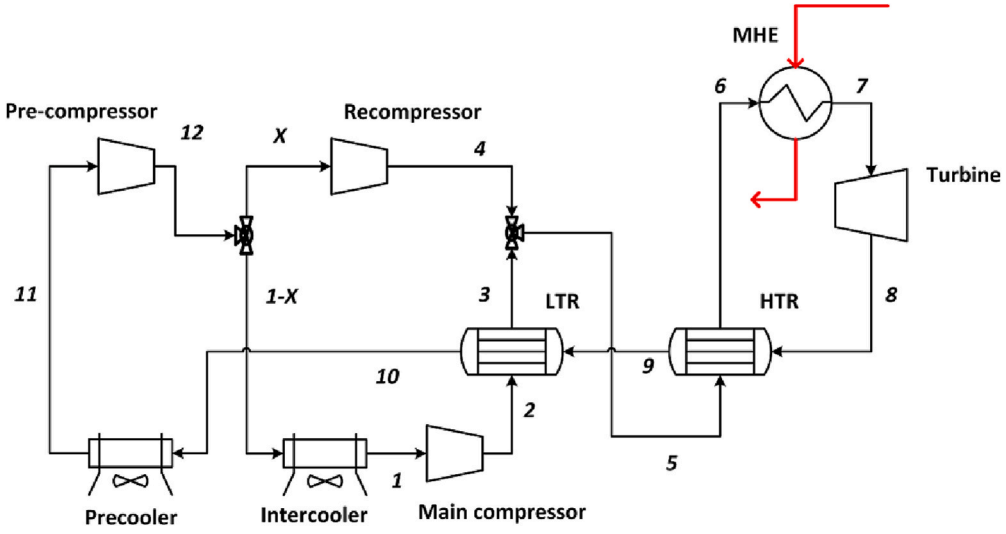

Fig. 2. Layout diagram of sCO_2 partial cooling cycle.

- Compression and expansion processes are adiabatic and non-isentropic. Isentropic efficiencies of compression process and expansion process are assumed to be 89% and 93% respectively as widely practiced in literature.
- The heat exchange between the environment and the system is neglected, except for the precooler/intercooler and dry cooler.
- In a partial cooling cycle configuration, the main compressor (state 1) and the precompressor (state 11) inlet temperatures are the same (or $T_{11} = T_1$).

The cold end temperature difference of the precooler/dry cooler/intercooler is assumed to be 15 K (i.e. $T_{min} - T_0 = 15$ K) [30]. This condition allows to control compressor inlet temperature (T_{min}) corresponding to variation in ambient air temperature (T_0).

Based on first principle of thermodynamics, energy balance is applied to each cycle component to compute power of turbomachinery (compressors and turbine) and heat duty of all heat exchangers (MHE and recuperators). Table 1 shows the governing equation for each cycle component and definition of cycle efficiency. Consumption of fan work in dry-cooler is significant so it is also incorporated in the definition of cycle efficiency.

To avoid pinch (or cross over of hot and cold streams), the log mean temperature difference (LMTD) of 15 K is fixed in dry cooler, precooler and intercooler. The required amount of air flow rate is calculated for every case to achieve the fixed LMTD.

Recuperator (HTR and LTR) in the cycles are printed circuit heat exchangers, therefore, minimum internal temperature difference (or pinch) in HTR and LTR is fixed at 10 K and 5 K respectively. To take into account the effect of pressure losses in heat exchangers, fractional pressure losses ($(P_{in} - P_{out})/P_{in}$) are considered as shown in Table 2.

2.3.2. Thermodynamic model validation

All thermodynamic calculations and cycle simulation are carried out using Aspen plus v11 software [31]. To ensure accuracy of the thermodynamic model, cycle simulation of sCO_2 recompression cycle is performed at same conditions as presented in Mohammadi et al. [32] (also reported in Table 3). The results obtained from Aspen Plus simulation are compared with the literature reference and presented in Table 4. As evident, a good agreement in cycle efficiency is obtained with a relative error of 1.52% which confirms the accuracy of the thermodynamic model.

Table 2
Fractional pressure loss in each heat exchanger of supercritical CO_2 cycle [10].

Heat Exchanger	Value
Recuperator hot side	1.5%
Recuperator cold side	0.5%
Main Heat Exchanger unit	1%
Precooler / dry cooler / intercooler	0.5%

Table 3
Reference parameters for thermodynamic model validation [32].

Parameters	Value	Remarks
Ambient/heat sink Temperature (T_0)	25 °C	
Ambient Pressure (P_0)	1.01 bar	
MC inlet Pressure (P_{min})	74 bar	
Pressure ratio of compressor (PR_c)	3	
Turbine inlet Temperature (T_{max})	550 °C	
Turbine isentropic efficiency (η_t)	0.9	
MC and RC isentropic efficiency (η_{mc} and η_{rc})	0.85	
MC inlet Temperature (T_{min})	35 °C	
Heat Source (Q_{MHE})	600 MW	
LTR and HTR effectiveness (ε_{LTR} and ε_{HTR})	0.86	Minimum internal temperature difference approach is used, MITA = 20 K

Table 4
Validation of thermodynamic simulation model of present work.

Parameters	Mohammadi et al [32] work	Present Work	Relative Error (%)
Turbine Work (MW)	414.2	414	0.04
Main Compressor Work (MW)	123.7	119.9	3.12
Recompressor Work (MW)	85.57	86.05	0.5
Net Work (MW)	204.9	208.1	1.5
Thermal Efficiency [%]	34.15	34.67	1.52

Table 1
Governing equations of thermodynamic model of each component of sCO_2 power cycle.

Component	Governing equations	
Heat duty of MHE	$\dot{Q}_{MHE} = \dot{m} \times (h_7 - h_6)$	
Turbine power	$\dot{W}_T = \dot{m} \times (h_7 - h_8)$	
Main Compressor power	$\dot{W}_{MC} = \dot{m} \times (1 - X) \times (h_2 - h_1)$	
Recompressor power (RC)	Recompression	$\dot{W}_{RC} = \dot{m} \times X \times (h_{11} - h_{10})$
	Partial Cooling	$\dot{W}_{RC} = \dot{m} \times X \times (h_4 - h_{12})$
Pre compressor power (PC)	$\dot{W}_{RC} = \dot{m} \times (h_{12} - h_{11})$	
Heat duty of HTR	$\dot{Q}_{HTR} = \dot{m} \times (h_8 - h_9)$	
Heat duty of LTR	$\dot{Q}_{LTR} = \dot{m} \times (h_9 - h_{10})$	
Heat duty Dry cooler	$\dot{Q}_{dc} = \dot{m} \times (1 - X) \times (h_{10} - h_1)$	
Heat duty Intercooler	$\dot{Q}_{ic} = \dot{m} \times (1 - X) \times (h_{12} - h_1)$	
Heat duty of Precooler	$\dot{Q}_{pc} = \dot{m} \times (h_{10} - h_{11})$	
Fan power [33]	$\dot{W}_{fan\ work} = 0.001.n_{fans}\left(\frac{\rho_{air}}{1.2}\right).\left(0.4762.\left(f_{airfan}\right)^2 - 59.4141.f_{airfan} + 186644\right)\frac{1}{\eta_{fan}}$	
Mass split fraction (X)	$X = \frac{\dot{m}_{recompressor}}{\dot{m}_7}$	
Cycle thermal efficiency	$\eta = \frac{\dot{W}_T - \dot{W}_C - \dot{W}_{fan\ work}}{\dot{Q}_H}$	

3. Response surface method

In this work, optimization and sensitivity study are carried out using the response surface method. In series of experiment generally one factor is dependent on another. One-factor at a time or trial and error approach is an inefficient and unstructured to find the optimum set of conditions of two or more process parameters. RSM is a combination of statistical and mathematical technique [34]. It could be used to analyze and optimize situations involving many inputs or choice variables that influence a dependent response variable. RSM models the association between choice variables and response variables, utilizing experimental designs such as factorial designs as input. A step by step procedure of response surface method adopted in this work is presented in Fig. 3.

The first step in RSM is to define the problem, which includes determining important variables and relevant system responses. The next and most crucial phase is experiment design. A full factorial design is used in this study to assess the model's accuracy before, after, and during the regression analysis. Full factorial design yields more information than other approaches at similar expense. Verifying the model's validity is the next step once the regression model has been developed. Following validation, statistical analysis (ANOVA) is used to determine the most important factor influencing the result. The next step is to choose the right balance to obtain the optimum response.

3.1. Choice of decision variables and response variable

In the present work, cycle thermal efficiency (η) is selected as the response variable since it describes the power block capability to convert thermal power into mechanical power and it also directly impacts the levelized cost of electricity (LCOE).

Three decision variables are selected for both cycle layouts: heat sink temperature or ambient air temperature (T_0), cycle minimum pressure (P_{min}) (*P_{min} represents the main compressor inlet pressure for recompression cycle and precompressor inlet pressure for partial cooling cycle*), and mass split fraction (X). The decision of range of decision variables is not random, rather it is decided on the basis of systematic review of recent studies which focused on optimization of cycle parameters of sCO_2 power cycles. Table 5 reports the values considered in the literature and the decided values used in this work.

The value for cycle minimum pressure, also known as compressor inlet pressure, ranges from 76 to 89 bar. Because the main goal is to investigate the effect of varying compressor inlet pressure close to CO_2 critical pressure, expanding the range to values >89 bar is not feasible. Finally, the mass split fraction range is decided to be 0.1 to 0.34 because this range has been used in previous works and values >0.34 result in infeasible results due to cross-over or very low pinch in the recuperators.

Cycle maximum pressure and maximum temperature are fixed at 250 bar and 680 °*C*; as these conditions are conveniently achievable in nuclear power plant, coal fired power plant and advanced CSP power plant using molten salt as heat transfer medium in thermal energy storage.

For full factorial experimental design, three levels of each decision variable are defined for both cycle configuration and experiments are carried out in Aspen Plus v11 simulation environment. The values of three levels are reported in Table 6.

4. Results and discussions

The results of numerical experiments performed in Aspen Plus v11 using the three levels of full factorial design are given in Appendix A. This section presents the results from analysis of full factorial design using RSM employing Minitab 20.3 software. This software calculates the coefficients of the regression model and also derive 3D plots and contours to study the effect of two or more decision variables on the desired response. In addition to RSM, analysis of variance (ANOVA) is employed to assess the appropriateness of the model and to decide the influencing parameters.

4.1. Regression model

The findings of the experiment with independent parameters and responses were fit to a polynomial equation, as stated below.

$$Y = B_o + \sum_{i=1}^{k} B_i x_i + \sum_{i=1}^{k} B_{ij} x_i^2 + \sum_{i=1}^{k-1} \sum_{j=2}^{k} B_{ij} x_i x_j.$$

Where Y is the predicted outcome. Constant, linear, quadratic, and interactive values of regression coefficients are assigned to B_o, B_i, B_{ii}, and B_{ij} respectively, X_i and X_j are input parameters, and i and j are index numbers. The generated regression equation calculates the impact of the input variables and their interactions. Based on the experimental methodology provided in Table 6, the RSM provides equation that characterize the effect of the examined factors on the cycle efficiency.

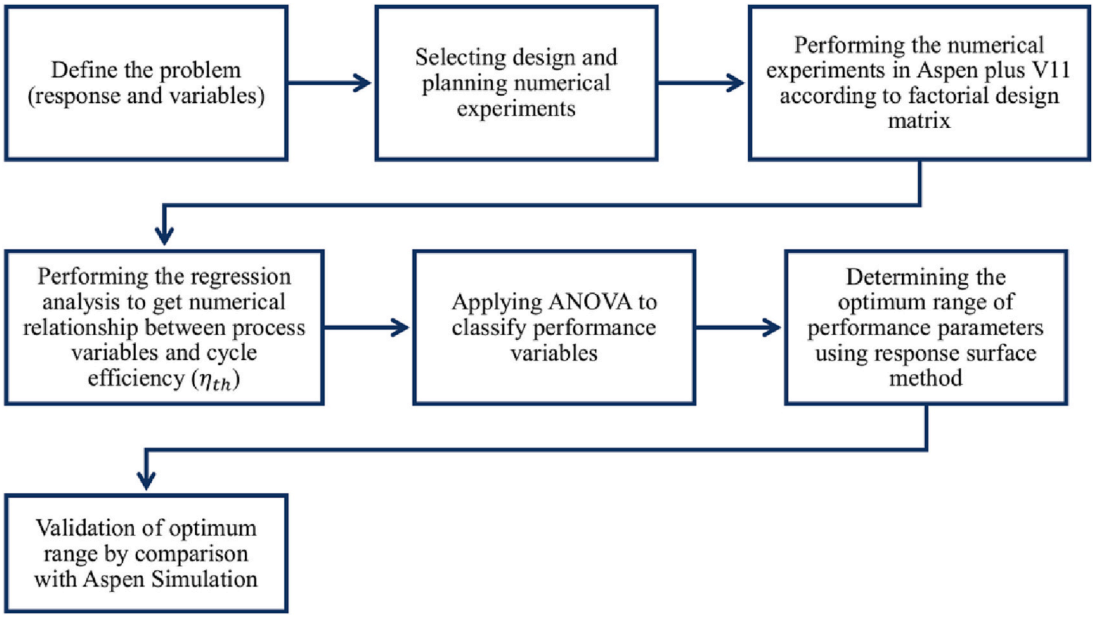

Fig. 3. Steps involved in response surface method for finding optimum and classification of performance parameters.

Table 5
Literature review to decide the range of cycle decision parameters for response surface method.

Parameters	Liu et al. [30]	Neises [35]	Li and Eri [13]	Chen et al. [36]	Salim et al. [37]	Reyes-Belmonte et al. [38]	Monjurul Ehsan et al. [39]	**This Work**
Main compressor inlet temperature [°C]	32–50	45	32–46	40–50	32–57	40	30–70	35–61
Main compressor/ Precompressor inlet pressure [bar]	76.3	55–65	74–88	78	74–90	78	80	76–89
Mass Split fraction (X)	0.39	0–0.4	–	0.25(Recompression cycle) 0.35 (Partial cooling cycle)	0.01–0.5	0.25	–	0.1–0.34
Pre-compressor outlet Pressure [bar]	–	80–105	77 (optimum)	99 (optimum)	–	–	90–140	110

Table 6
Decision variables with their levels for full factorial design.

Factors	Decision Variable	Low level	Mid-level	High level	Recompression cycle	Partial cooling cycle
1	Main compressor inlet / precompressor inlet or cycle minimum pressure [bar], P_{min}	76	82.5	89	✓	✓
2	Heat sink temperature [°C], T_o	20	33	46	✓	✓
3	Mass split fraction, X	0.1	0.22	0.34	✓	✓

As a result of RSM, the following mathematical models of the thermodynamic efficiency of both types of cycle configurations are obtained:

$$\eta_{recomp} = 0.691 + 0.0039P_{min} - 0.00374T_0 + 0.094X - 0.000002{P_{min}}^2 - 0.000029{T_0}^2 - 1.185X^2 + 0.000076P_{min}T_0 + 0.00990P_{min}X - 0.01089T_0X$$

$$\eta_{PC} = 1.328 - 0.0200P_{min} - 0.00393T_0 + 0.468X - 0.000093{P_{min}}^2 - 0.000088{T_0}^2 - 0.007X^2 + 0.000125P_{min}T_0 + 0.00495P_{min}X - 0.00084T_0X$$

R^2 values are calculated to ensure that the data fits well together. For the perfect fit of data, its value spans from zero to one. The R^2 values of the developed models for the recompression and partial cooling cycles are 0.9421 and 0.8925, respectively, showing a good fit to the data. The adjusted R^2 value, on the other hand, also show the model's accuracy with values between 0 and 1; The adjusted R^2 for the recompression cycle model is 0.9114, whereas the adjusted R^2 for the partial cooling cycle model is 0.8356, indicating acceptable model accuracy.

Table 7
Experimental and predicted results for recompression and partial cooling cycle.

Run no.	P_{min}	T_0	X		Recompression cycle efficiency	Partial cooling cycle efficiency
1	89	46	0.1	Aspen Plus	0.4375	0.441
				Predicted	0.4408	0.446
				Relative Error	0.754%	1.134%
2	76	20	0.34	Aspen Plus	0.4864	0.477
				Predicted	0.4874	0.467
				Relative Error	0.206%	2%
3	76	46	0.1	Aspen Plus	0.4334	0.444
				Predicted	0.4374	0.439
				Relative Error	0.923%	1.12%

To validate the RSM, the model equation for predicting optimal response values is assessed under the specified conditions. Three confirmation experiments were carried out to validate the mathematical models, using process parameters chosen at random from the ranges presented in Table 6. Table 7 shows the actual values from Aspen Plus simulation, predicted values from the model, and percentage error in the experiments. A good agreement between Aspen Plus simulation and regression model confirms the model's validity for both recompression and partial cooling layouts (See Table 7).

4.2. Identification of significant parameters

Analysis of variance (ANOVA) is a statistical tool for identifying the most significant process variables that influence output values. The ANOVA computes values such as F-value (F) and p-value (p) that were used to establish the model's significance, as illustrated in Table 8 and Table 9.

The F-value in ANOVA shows the variation within the sample. The greater the F-value, the greater the dispersion in samples as compared to

Table 8
Analysis of Variance for recompression sCO_2 cycle.

Source	F-Value	P-Value	Significance
Model	30.71	0	
Linear	54.83	0	$p < 0.05$, significant
T_0	158	0	
P_{min}	2.62	0.124	$p > 0.05$, less-significant
X	3.87	0.066	
2-Way Interaction	26.57	0	
$P_{min} \times T_0$	8.52	0.01	$p < 0.05$, significant
$P_{min} \times X$	12.18	0.003	
$X \times T_0$	59.01	0	

Table 9
Analysis of Variance for partial cooling sCO_2 cycle.

Source	F-Value	P-Value	Significance
Model	15.69	0	
Linear	31.02	0	
P_{min}	34.69	0	
X	34.48	0	$p < 0.05$, significant
T_0	23.9	0	
2-Way Interaction	8.28	0.001	
$P_{min} \times T_0$	21.6	0	
$P_{min} \times X$	2.9	0.107	$p > 0.05$, less-significant
$X \times T_0$	0.33	0.57	

variance within samples.

p-value is calculated using the F-value, which is used to determine the statistical significance of the terms and model. The *p*-value is a probability that compares evidence to the null hypothesis. Lower probability provides more evidence to support the null hypothesis. A significance level of 0.05 is selected in our study represents a 5% chance of finding that there is a relationship. If the p-value is <0.05, the process parameter is said to be significant; otherwise, it is said to be less-significant.

The ANOVA results in Table 8 and Table 9 show that the heat sink temperature is the most effective parameter for recompression and partial cooling cycles because it has a low p-value ($p < 0.05$) and a high

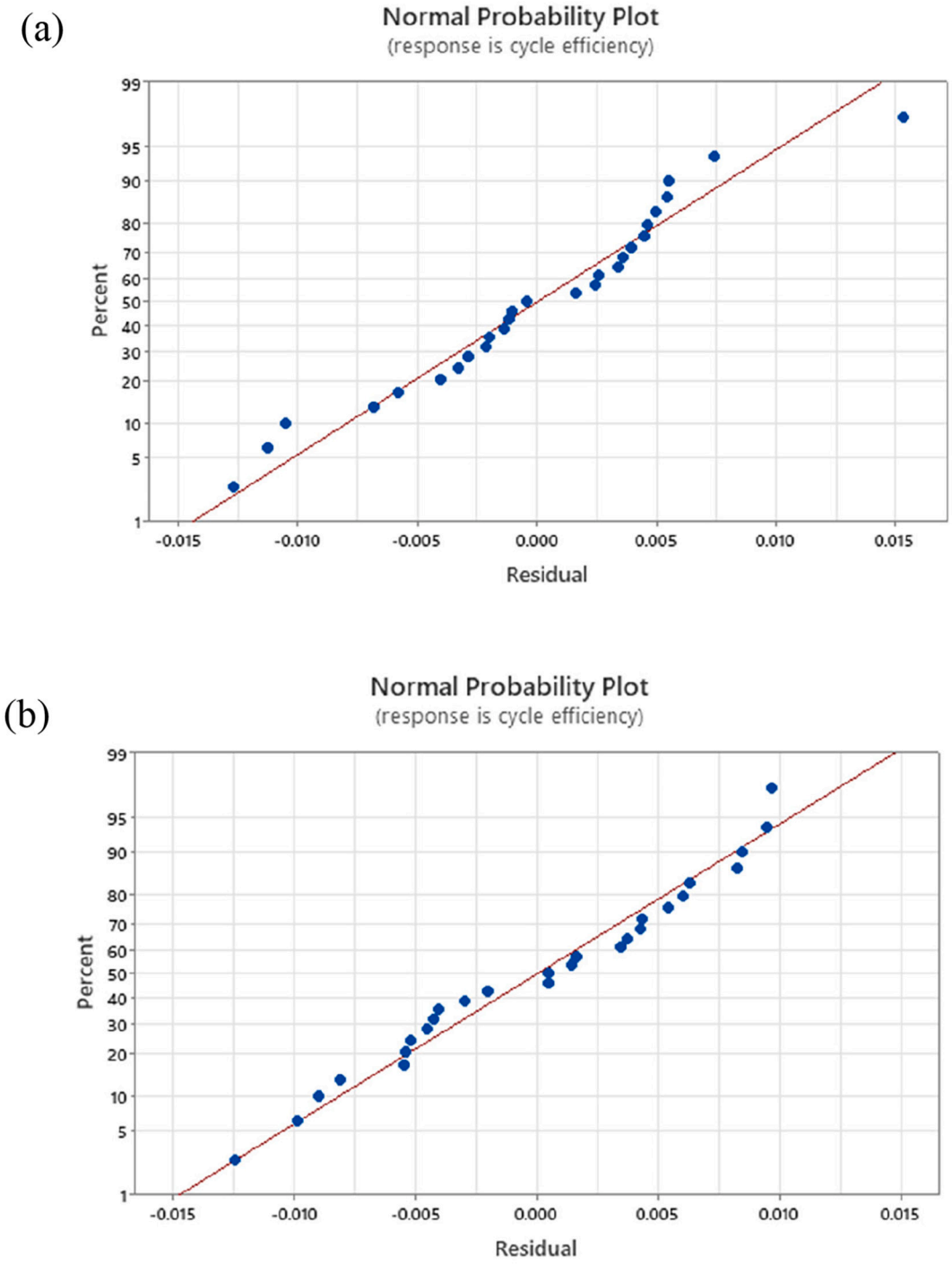

Fig. 4. Normal Probability Plot for response variable (a) recompression cycle (b) partial cooling cycle.

F-value. In the recompression cycle, the temperature of the heat sink is the most significant parameter, followed by the mass split fraction (X) whereas contribution of minimum pressure on cycle efficiency is less significant. In the partial cooling cycle, the minimum pressure is the most important parameter, followed by the mass split fraction and heat sink temperature based on their low *p*-values and higher F-values.

The p-value for decision variables, as well as their one-way and two-way relationships in both the recompression and partial cooling supercritical sCO_2 cycles, are summarized in Table 8 and Table 9. The normal probability plot assesses the roughly normal distribution of the residuals. It is one of the most important criteria for establishing the validity of ANOVA. Fig. 4 (a) and (b) show that the residuals for sCO_2 thermal efficiency follow a normal distribution in both the recompression and partial cooling cycles.

The Pareto chart is a visual representation of data that is used to prioritize the importance of factors affecting a response. In the context of Response Surface Methodology (RSM) and Analysis of Variance (ANOVA), the Pareto chart is used to identify the most significant factors affecting the response, so that further experimentation and optimization can be focused on these factors. Therefore, Pareto chart [40] is prepared to evaluate and analyze the magnitude of the effects of various variables on the response. A reference line is drawn and the effects are placed on the chart in decreasing order of the absolute value of standardized effects. The input impact Pareto bar of all parameters to the right of the vertical red line is statistically significant, as shown in Fig. 5 (a) and (b). A pareto chart arranges the length of each bar based on its standardized effect.

4.3. Optimum point

The response optimizer identifies the set of input variable that optimizes one or more responses. Fig. 6 and Fig. 7 show the input variable values that maximize cycle thermal efficiency obtained from the developed model using the response optimizer. The global optimal combination for the recompression cycle is a heat sink temperature of 20 $^{\circ}C$, a mass split fraction of 0.3182, and a minimum pressure of 89 bar to achieve the highest cycle thermal efficiency of 0.4963. In similar way, the global optimal combinations for a partial cooling cycle are: 32.8$^{\circ}C$

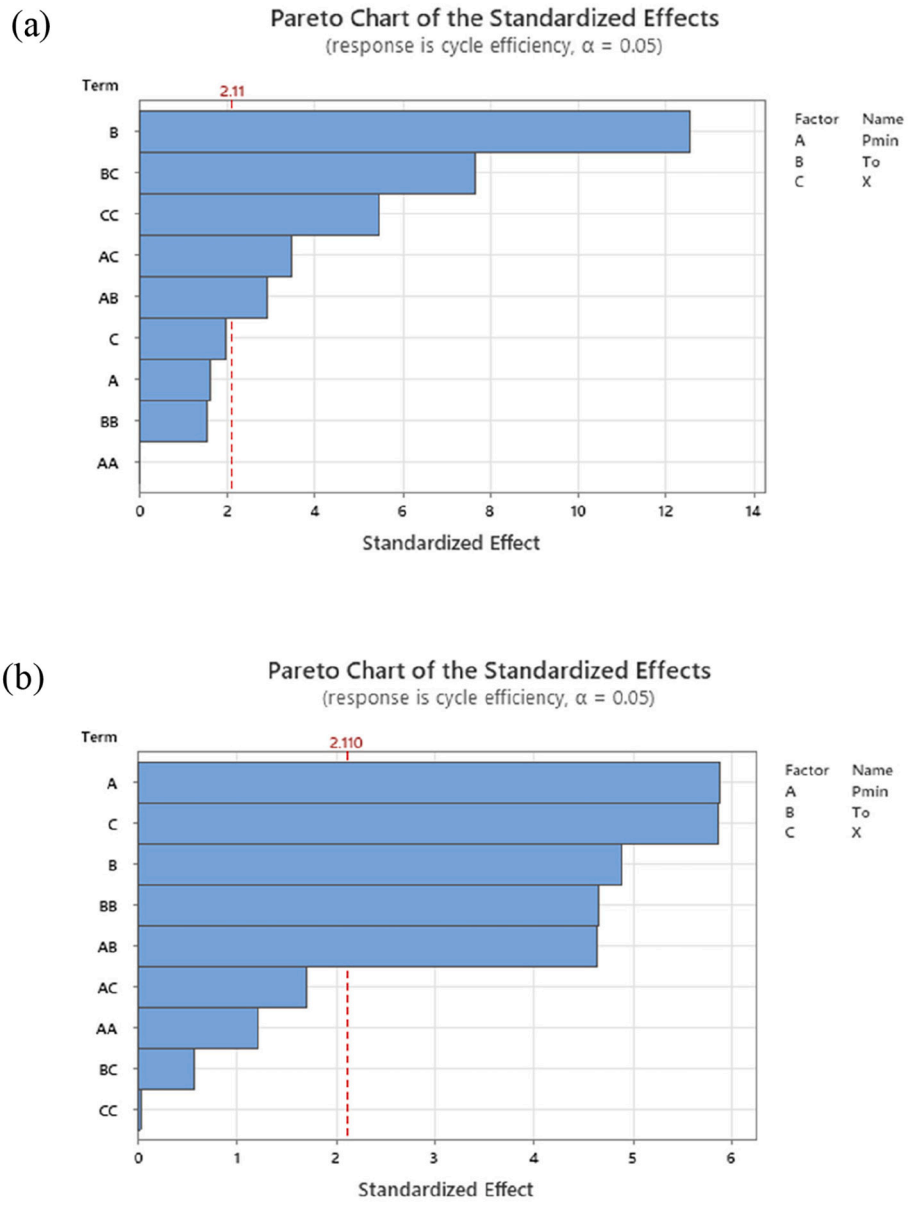

Fig. 5. Pareto Chart of the Standardized effects (a) recompression cycle (b) partial cooling cycle.

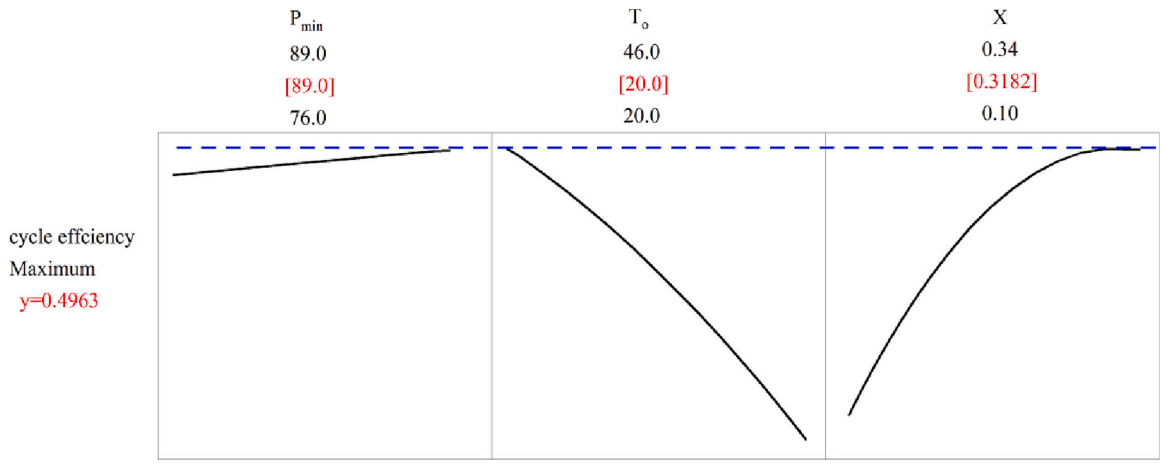

Fig. 6. Global optimum point of recompression cycle.

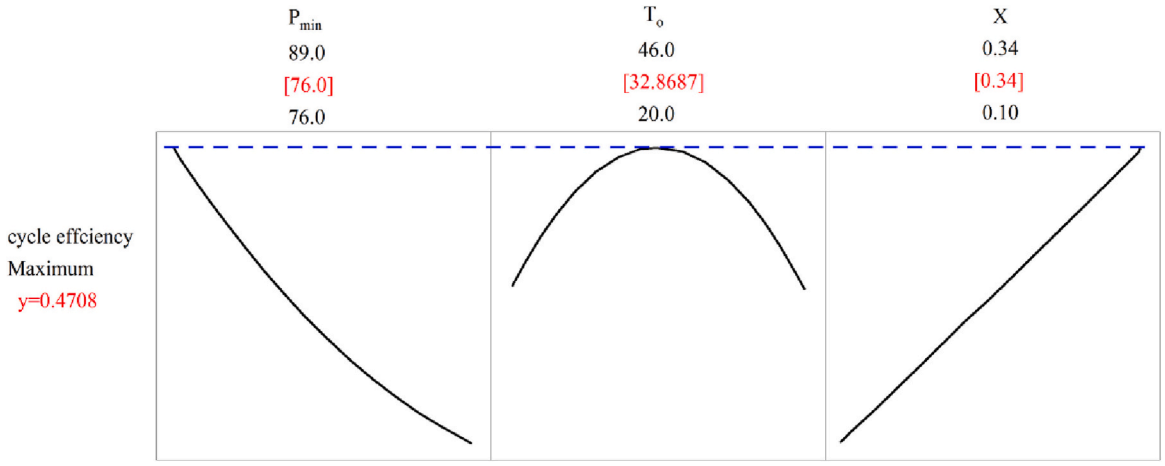

Fig. 7. Global optimum point of partial cooling cycle.

heat sink temperature, mass split fraction of 0.34, minimum pressure of 76 bar, that results in a cycle thermal efficiency of 0.4708.

4.4. Influence of heat sink temperature (T_0) and cycle minimum pressure (P_{min})

4.4.1. Recompression cycle

Fig. 8a and Fig. 8b demonstrates the influence of heat sink temperature (or ambient air temperature) in dry cooler (T_0) and cycle minimum pressure (P_{min}) on cycle thermal efficiency for recompression and partial cooling cycles keeping mass split fraction constant at optimum value determined in the previous section. The main reason of studying contour plots is to observe the trend of cycle efficiency and to figure out which cycle configuration is more sensitive to rise in ambient temperature and cycle minimum pressure.

For recompression sCO_2 cycle, cycle efficiency drops from 0.492 to 0.405 (8.7 points) with increase in heat sink temperature in dry-cooler from 20°*C* to 46°*C* (keeping compressor inlet pressure or P_{min} equal to 76 bar) as shown in Fig. 8a. It means, the sCO_2 recompression cycle operating in high temperature zones for example installation in desert areas with higher ambient air temperature, the cycle efficiency drops by 8.7 points which significantly impacts the cost of electricity compared to operation of cycle in cold areas with lower heat sink temperatures.

In thermodynamic point of view, as the compressor inlet temperature increases, the compressibility factor also increases compared to compressibility factor (Z) at temperature close to critical point (31°*C*). Owing to increase in compressibility factor at compressor inlet, compressor work consumption increases which in turn decreases cycle thermal efficiency. This effect is also pointed out earlier in literature [41–43].

Fig. 8a reveal that the cycle efficiency at higher heat sink temperatures can be improved by increasing the cycle minimum pressure (P_{min}). Because, an increase in P_{min} along with an increase in T_0 results in higher density at the compressor inlet, which results in lower compression work and increase in cycle efficiency. However, an increase in P_{min} also results in a decrease in pressure ratio across the turbine that leads to lower turbine work. Therefore, values of cycle minimum pressure larger than 89 bar are not considered in the analysis. At constant T_0 for example 46 °*C*, the rise in P_{min} (moving horizontally in contour plot) results in improvement in cycle efficiency of recompression cycle from 0.405 to 0.437 (3.2 points).

Considering P_{min} of 89 bar, the cycle efficiency drops from 0.497 to 0.436 (6.1 points) for increase in T_0 from 20 to 46 °*C*. It means, at higher P_{min}, the drop-in cycle efficiency is less sensitive to T_0 compared to efficiency drop at lower cycle minimum pressure (value close to 76 bar).

4.4.2. Partial cooling cycle

The trend of cycle efficiency with variation in T_0 and P_{min} in case of partial cooling cycle is quite different from recompression cycle (see Fig. 8b). In partial cooling cycle, for P_{min} of 76 bar, cycle efficiency increases from 0.459 to 0.4746with rise in heat sink temperature from 20 to 34 °C followed by decrease in cycle efficiency from 0.4746to 0.4603

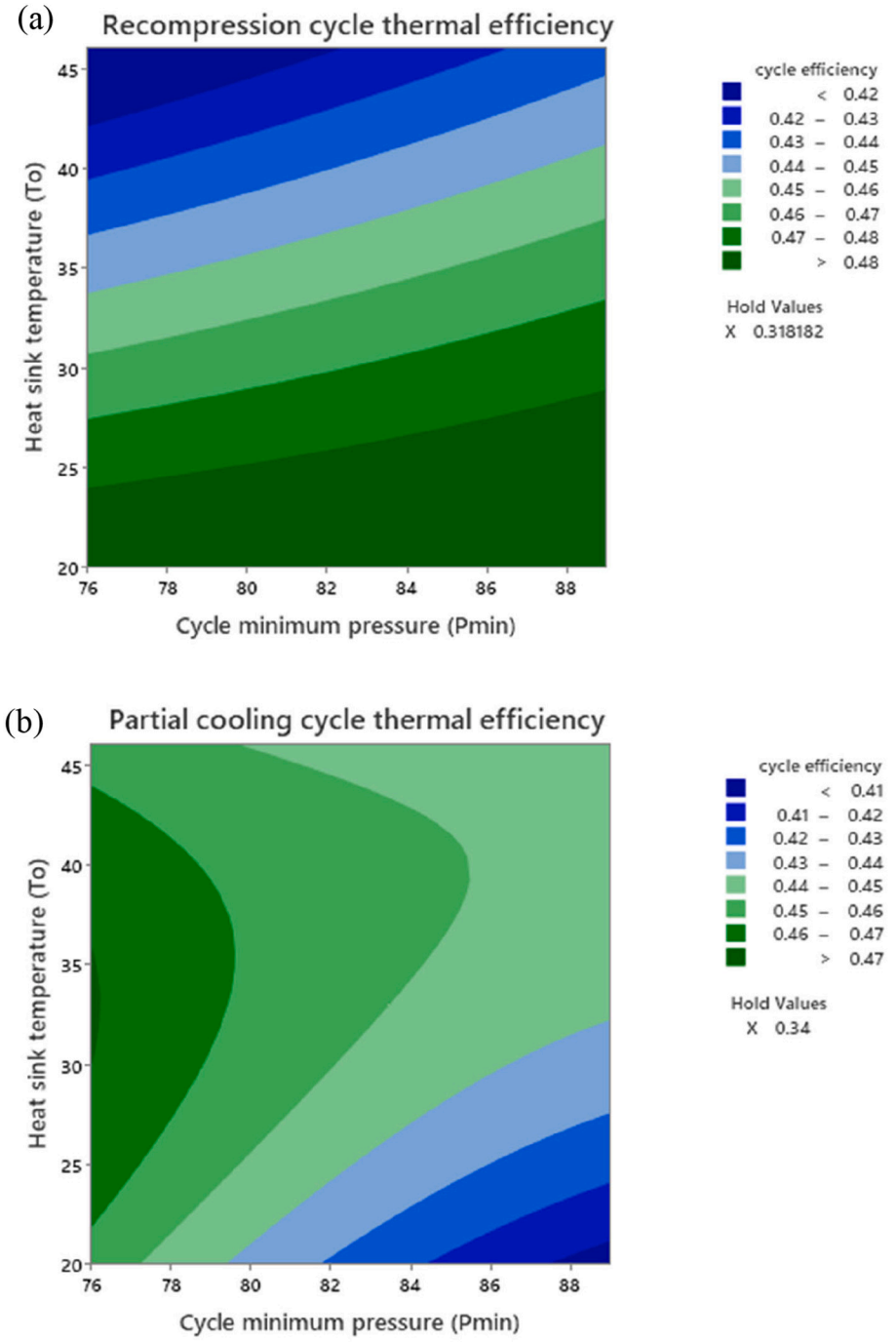

Fig. 8. Interaction effect of heat sink and minimum pressure on cycle thermal efficiency (a) Recompression cycle (b) Partial cooling cycle.

with rise in T_0 from 34 to 46°*C*. The first increase in trend of cycle efficiency is due to decrease in thermal power input in MHE which is more dominant than rise in compressor power due to T_0. However, for higher T_0, the rise in compressor power become dominant due to which drop in cycle efficiency is observed according to the definition of cycle efficiency (Fig. 9 demonstrate that the heat transfer rate in MHE decreases from 110 to 105.9 MW with rise in heat sink temperature from 20 to 34 °C to maintain constant net power output of 50 MW). Moreover, in partial cooling cycle, the rise in P_{min} does not enhance cycle efficiency owing to reduction of expansion power in turbine. At T_0 of 46 °*C*, the increase in P_{min} from 76 to 89 bar results in reduction of cycle efficiency from 0.4603 to 0.4527 (0.76 points).

Results also show that cycle efficiency is more sensitive to rise in T_0 at higher values of P_{min} in partial cooling cycle compared to trend for smaller values of P_{min}. Unlike the decreasing trend in recompression cycle, the cycle efficiency improves from 0.409 to 0.4527 (4.37 points) with increase in T_0 from 20 to 46°*C* at P_{min} of 89 bar in partial cooling cycle. (read Fig. 8b moving vertically upward in contour chart). This trend of increasing cycle efficiency is also attributed to a decrease in MHE heat transfer rate (See Fig. 9) while maintaining a constant cycle net power output of 50 MW.

4.5. *Influence of heat sink temperature (T_0) and mass split fraction (X)*

Fig. 10 a and b show the effect of the heat sink temperature (T_0) and mass split fraction (X) on cycle efficiency of sCO_2 recompression and

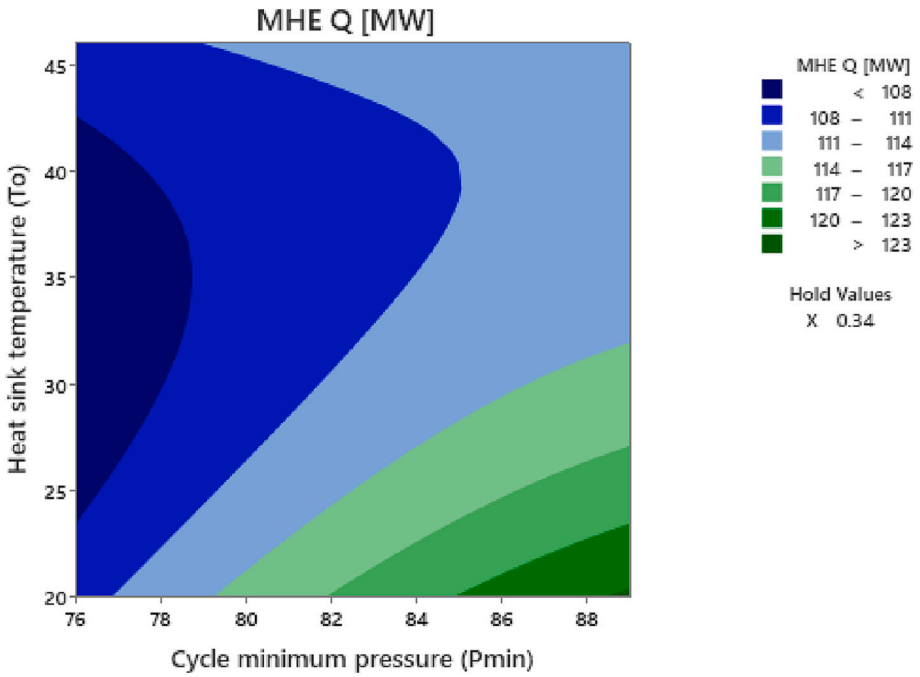

Fig. 9. Interaction effect of heat sink and minimum pressure on main heat exchanger heat transfer rate for partial cooling cycle.

partial cooling cycle keeping P_{min} constant at the optimum value. The mass split fraction refers to the amount of flow bypassed to the Recompressor. It is also important to study the effect of varying mass split fraction on cycle efficiency and to find the optimum range at higher heat sink temperature (T_0).

The reason of introducing mass split in sCO_2 cycles is to enhance heat recovery in recuperators by varying the mass flow rates between hot and cold streams inside the recuperator. The difference of mass flow brought about balance between heat capacities ($\dot{m}C_p$) of two streams which enhances heat recuperation and improves recuperator effectiveness [44,45]. In this section, sensitivity of mass split and ambient air temperature to cycle efficiency is investigated and optimum range of mass split is decided to achieve higher cycle thermal efficiency.

4.5.1. Recompression cycle

Fig. 10a illustrate the contours of cycle efficiency subject to variation in X and T_0 for recompression cycle. At a constant heat sink temperature of 20 °C, the cycle efficiency increases from 0.4408 to 0.4974 (5.66 points). However, at a higher heat sink temperature of 35 °C, the cycle efficiency is maximized at a mass split fraction of 0.24. The bending of contour curves indicates that the optimal range of mass split X decreases as T_0 increases.

4.5.2. Partial cooling cycle

The effect of mass split fraction X and T_0 on the cycle efficiency of partial cooling cycle is shown in Fig. 10b. In the case of partial cooling cycle, with an increase in mass split fraction X from 0.1 to 0.34, cycle efficiency increases from 0.445 to 0.474 (2.9 points) at a constant heat sink temperature of 35 °C. Overall, the cycle efficiency of partial cooling cycle is less sensitive to rise in mass split fraction X compared to effect observed in the recompression cycle.

As a final step in the analysis, at optimum point of two power cycles, power balance is reported in Table 10 for 50 MW output of power cycle. Moreover, the cycle process diagram at optimum conditions are shown in Fig. 11 and Fig. 12 for Recompression and Partial cooling cycle respectively. These diagrams are helpful to study the temperature differences across heat exchangers and temperature rise and drop in turbomachinery.

5. Conclusion

The primary goal of this work is to investigate the effects of dry cooler heat sink temperature, mass split fraction, and cycle minimum pressure on the thermal efficiency of sCO_2 recompression and sCO_2 partial cooling cycles. The process begins by utilizing the Response Surface Method (RSM) to construct a model of the cycle thermal efficiency. The optimal ranges of cycle decision parameters are then determined. Finally, a performance study is performed to assess the sensitivity of cycle thermal efficiency to changes in cycle decision parameters. The optimization and performance study revealed the following key findings:

- Full factorial design is selected in RSM and second order regression model is developed to predict cycle efficiency of the two sCO_2 power cycles. The data for full factorial design is derived from numerical simulations performed in Aspen plus V11.
- Analysis of variance (ANOVA) provides the statistical significance of selected decision parameters on the basis of *p*-value and F-value. In Recompression cycle, the most significant parameter is T_{min}, mass split fraction X is second most significant and P_{min} is the third most significant parameter. However, in Partial cooling cycle, the order of significance of parameters is P_{min}, mass split fraction X and then T_{min}.
- For the recompression cycle, the global optimal combination is found at a heat sink temperature of 20 °C, a recompressor mass fraction of 0.3182, and a minimum pressure of 89 bar to obtain the highest thermal efficiency of 0.4963. For a partial cooling cycle, the global optimal combination is found at a dry cooler temperature of 32.8 °C, recompressor mass fraction of 0.34, and minimum pressure of 76 bar to yield cycle thermal efficiency of 0.4708.
- Thermodynamic sensitivity of recompression sCO_2 cycle for varying T_0 and P_{min} is also performed. At P_{min} of 76 bar, the rise in T_{min} results in 8.7 points decrease in cycle thermal efficiency. However, to reduce the sensitivity of cycle thermal efficiency, increase in P_{min} is suggested. If P_{min} in increase to 89 bar, the drop in efficiency with rise in T_0 become smaller (i.e. 6.1 points).
- Unlike the decreasing trend in recompression cycle, the cycle efficiency improves from 0.409 to 0.4527 (4.37 points) with increase in T_0 from 20 to 46°*C* at P_{min} of 89 bar in Partial cooling cycle.

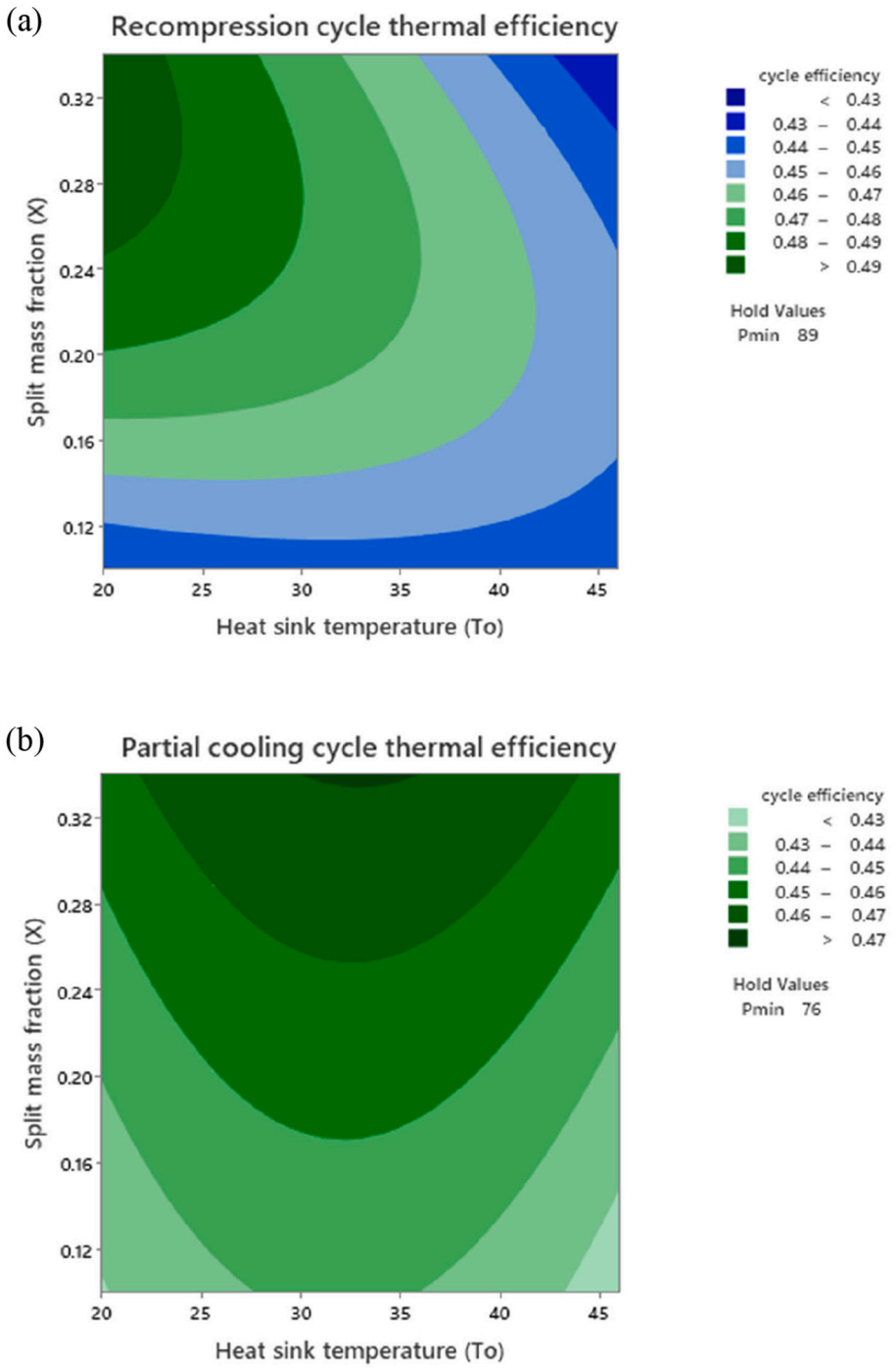

Fig. 10. Interaction effect of heat sink and recompressor mass fraction on cycle thermal efficiency (a) Recompression cycle (b) Partial cooling cycle.

- In Recompression cycle, the rise in mass split fraction X produces rise in cycle efficiency i.e. 5.66 points at optimum T_0 and P_{min}. However, the optimum range of split fraction X is different corresponding to different cycle minimum temperature (or different T_0).
- In partial cooling cycle, the cycle thermal efficiency is less sensitive to increase in split fraction X (i.e. 2.9 points efficiency rise) than the recompression cycle layout.

In present study, RSM (a combination of mathematical and statistical techniques) is adopted to generate a regression model of the relationship between the cycle thermal efficiency and cycle decision parameters. Furthermore, it identifies the most significant cycle parameters as well as their range of values for an optimum solution. In future, it is decided to include also other cycle parameters in optimization study like cycle maximum pressure, cycle maximum temperature and turbomachinery efficiency parameters and find optimum conditions for other advanced cycle layouts like Pre-compression cycle and Recompression with reheat cycle. In order to get a better decision on optimum set of parameters, neural network technique could be useful.

Table 10
Power balance of two sCO_2 cycles at optimum condition for 50 MW power output.

Cycle parameter	Recompression cycle	Partial Cooling cycle
Main Compressor power [MW]	7.47	6.65
Recompressor power [MW]	8.44	6.09
Pre-compressor power [MW]	0	6.06
Turbine power [MW]	67.57	69.84
Fan power [MW]	1.66	1.02
Heat duty of LTR	65.94	30.96
Heat duty of HTR	174.35	161.62
Heat duty of MHE	100.50	107.20
Heat duty of Precooler	0	28.24
Heat duty of Dry cooler	48.45	27.66
Cycle Thermal Efficiency	0.4975	0.4664

Nomenclature

Acronyms

sCO_2	Supercritical CO_2
RSM	Response surface method
ANOVA	Analysis of variance
IEA	International energy agency
LCOE	Levelized cost of electricity
CSP	Concentrated solar power plants
TIT	Turbine inlet temperature
LTR	Low temperature recuperator
HTR	High temperature recuperator
MHE	Main heat exchanger unit

P	Pressure, bar
PR	Pressure ratio
T	Temperature

Greek Symbols

ϵ	Effectiveness of recuperator
$\dot{m}$	Mass flow rate
$\dot{W}$	Power output of turbomachinery
X	Mass split fraction/fraction of mass flow towards Recompressor.
η	Thermal efficiency
f_{airfan}	Maximum flow of air per fan
η_{fan}	Efficiency of fan (0.9)
ρ_{air}	Air density, kg/m^3
n_{fans}	Number of fans

Subscripts

c	Compressor
LTR	Low temperature recuperator
HTR	High temperature recuperator
max	Maximum or turbine inlet
min	Minimum or compressor inlet
ic	intercooler
mc	Main compressor
rc	Recompressor
0	Ambient
t	Turbine

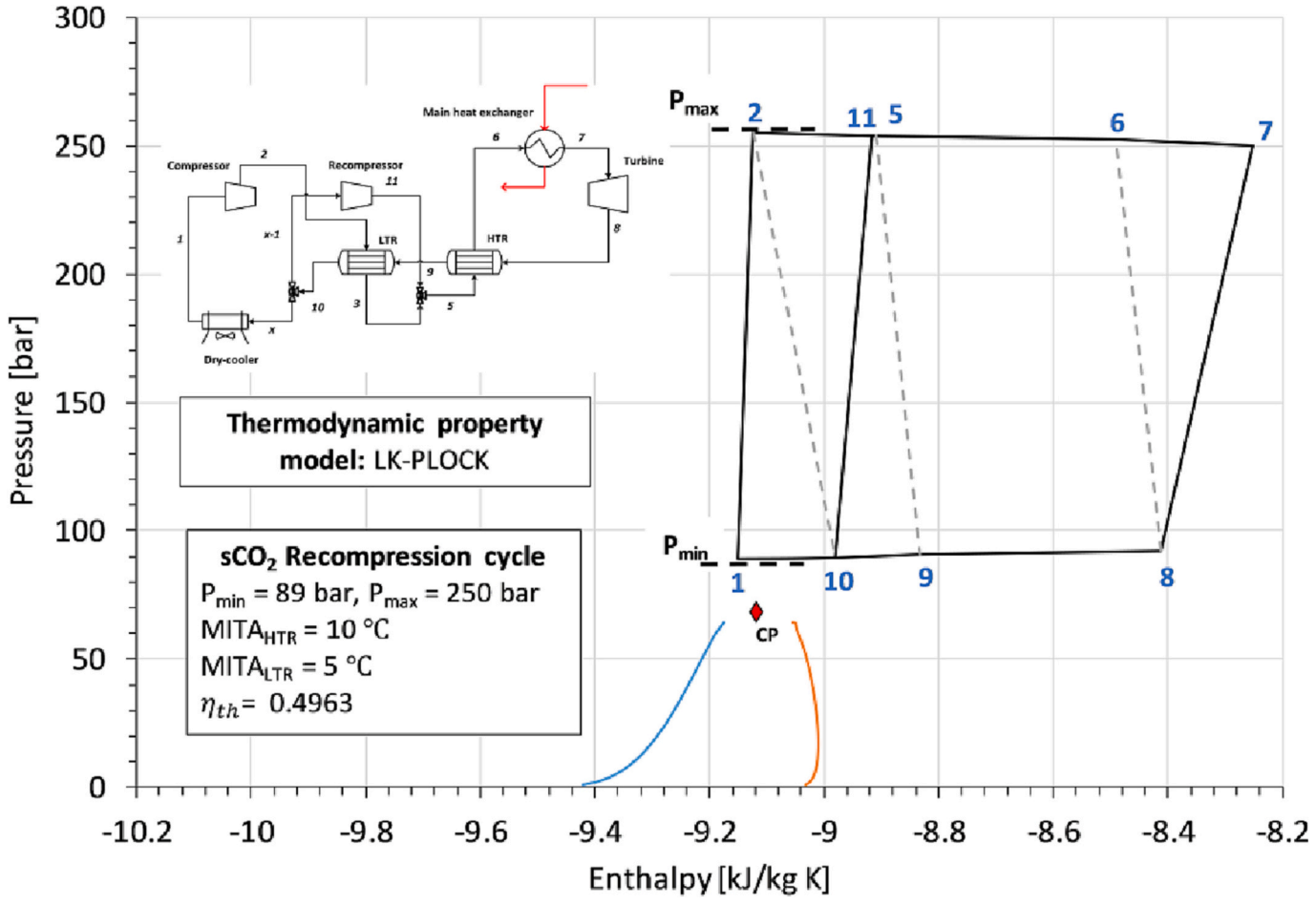

Fig. 11. Cycle process diagram of Recompression sCO_2 cycle at optimum conditions.

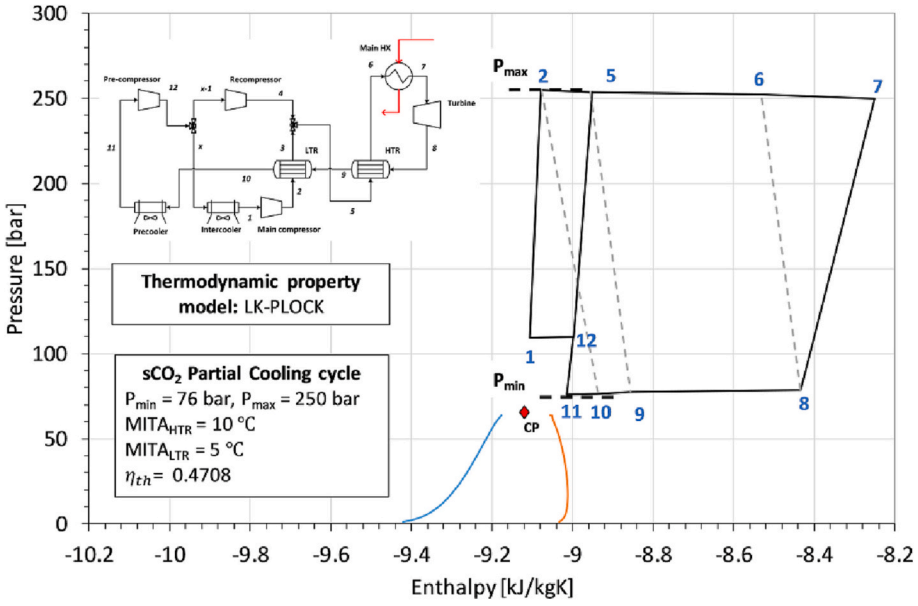

Fig. 12. Cycle process diagram of sCO_2 Partial cooling cycle at optimum conditions.

CRediT authorship contribution statement

Muhammad Ahmed: Methodology, Software, Validation, Formal analysis, Investigation, Data curation, Writing – original draft, Writing – review & editing, Visualization. **Abubakr Ayub:** Methodology, Software, Validation, Formal analysis, Investigation, Data curation, Writing – original draft, Writing – review & editing, Visualization. **Nadeem Ahmed Sheikh:** Conceptualization, Methodology, Validation, Investigation, Resources, Writing – original draft, Writing – review & editing, Visualization, Supervision, Project administration, Funding acquisition. **Muhammad Wakil Shahzad:** Supervision, Project administration, Funding acquisition, Writing – review & editing, Investigation. **Muhammad Haroon:** Conceptualization, Methodology, Validation, Investigation, Resources, Writing – original draft, Writing – review & editing, Visualization, Supervision, Project administration, Funding acquisition. **Muhammad Imran:** Conceptualization, Methodology, Validation, Investigation, Resources, Writing – original draft, Writing – review & editing, Visualization, Supervision, Project administration, Funding acquisition.

Declaration of Competing Interest

The authors declare that they have no known competing financial interests or personal relationships that could have appeared to influence the work reported in this paper.

Data availability

Data will be made available on request.

Appendix A. Appendix

P_{min}	T_o	X	Recompression sCO_2 cycle thermal efficiency from Aspen plus Simulation	Partial cooling cycle sCO_2 cycle thermal efficiency from Aspen Plus Simulation
89	46	0.1	0.437	0.425
82.5	46	0.1	0.433	0.429
89	20	0.22	0.472	0.401
82.5	20	0.1	0.449	0.403
76	20	0.1	0.466	0.433
89	20	0.34	0.501	0.401
82.5	20	0.22	0.477	0.409
82.5	33	0.22	0.475	0.445
89	33	0.22	0.476	0.438
82.5	46	0.34	0.412	0.449
89	33	0.1	0.452	0.425
76	20	0.34	0.486	0.466
76	46	0.22	0.439	0.440
76	20	0.22	0.490	0.451
76	33	0.22	0.473	0.447
89	33	0.34	0.465	0.451
89	46	0.22	0.456	0.433
76	46	0.34	0.399	0.453
82.5	46	0.22	0.447	0.439
89	46	0.34	0.426	0.443
76	33	0.34	0.436	0.465
82.5	33	0.1	0.451	0.431
82.5	20	0.34	0.507	0.414

(*continued on next page*)

(*continued*)

P_{min}	T_o	X	Recompression sCO_2 cycle thermal efficiency from Aspen plus Simulation	Partial cooling cycle sCO_2 cycle thermal efficiency from Aspen Plus Simulation
82.5	33	0.34	0.450	0.461
76	46	0.1	0.433	0.429
89	20	0.1	0.442	0.400
76	33	0.1	0.452	0.431

References

[1] L. Cozzi, T. Gould, World Energy Outlook 2021, IEA Publ, 2021, pp. 1–386 [Online]. Available: www.iea.org/weo.

[2] S. Khatoon, S. Ishaque, M.H. Kim, Modeling and analysis of air-cooled heat exchanger integrated with supercritical carbon dioxide recompression Brayton cycle, Energy Convers. Manag. 232 (January) (2021) 113895, https://doi.org/10.1016/j.enconman.2021.113895.

[3] Z. Yang, Y. Le Moullec, J. Zhang, Y. Zhang, Dynamic modeling of 5 MWe supercritical CO2 recompression Brayton cycle, AIP Conf. Proc. 2033 (November) (2018), https://doi.org/10.1063/1.5067089.

[4] M.T. White, G. Bianchi, L. Chai, S.A. Tassou, A.I. Sayma, Review of supercritical CO2 technologies and systems for power generation, Appl. Therm. Eng. 185 (Feb. 2021) 116447, https://doi.org/10.1016/j.applthermaleng.2020.116447.

[5] L. Sun, D. Wang, Y. Xie, Thermodynamic and exergoeconomic analysis of combined supercritical CO2 cycle and organic Rankine cycle using CO2-based binary mixtures for gas turbine waste heat recovery, Energy Convers. Manag. 243 (2021), 114400, https://doi.org/10.1016/j.enconman.2021.114400.

[6] A. Ayub, N.A. Sheikh, R. Tariq, M.M. Khan, C.M. Invernizzi, Exergetic optimization and comparison of combined gas turbine supercritical CO 2 power cycles, J. Renew. Sustain. Energy 10 (4) (Jul. 2018) 044703, https://doi.org/10.1063/1.5038333.

[7] M. Marchionni, G. Bianchi, S.A. Tassou, Techno-economic assessment of joule-Brayton cycle architectures for heat to power conversion from high-grade heat sources using CO2 in the supercritical state, Energy 148 (Apr. 2018) 1140–1152, https://doi.org/10.1016/j.energy.2018.02.005.

[8] M. Monjurul Ehsan, Z. Guan, A.Y. Klimenko, X. Wang, Design and comparison of direct and indirect cooling system for 25 MW solar power plant operated with supercritical CO2 cycle, Energy Convers. Manag. 168 (February) (2018) 611–628, https://doi.org/10.1016/j.enconman.2018.04.072.

[9] Y. Ma, T. Morosuk, J. Luo, M. Liu, J. Liu, Superstructure design and optimization on supercritical carbon dioxide cycle for application in concentrated solar power plant, Energy Convers. Manag. 206 (November 2019) (2020) 112290, https://doi.org/10.1016/j.enconman.2019.112290.

[10] G. Manente, F.M. Fortuna, Supercritical CO2 power cycles for waste heat recovery: a systematic comparison between traditional and novel layouts with dual expansion, Energy Convers. Manag. 197 (July) (Oct. 2019) 111777, https://doi.org/10.1016/j.enconman.2019.111777.

[11] F. Crespi, G. Gavagnin, D. Sánchez, G.S. Martínez, Supercritical carbon dioxide cycles for power generation: a review, Appl. Energy 195 (Jun. 2017) 152–183, https://doi.org/10.1016/j.apenergy.2017.02.048.

[12] E. Wang, N. Peng, M. Zhang, System design and application of supercritical and Transcritical CO2 power cycles: a review, Front. Energy Res. 9 (November) (2021) 1–20, https://doi.org/10.3389/fenrg.2021.723875.

[13] C. Li, Q. Eri, Comparative study of three modified sCO2 Brayton recompression cycles based on energy and exergy analysis with GA optimisation, Int. J. Exergy 35 (2) (2021) 241, https://doi.org/10.1504/IJEX.2021.115652.

[14] T. Neises, C. Turchi, A comparison of supercritical carbon dioxide power cycle configurations with an emphasis on CSP applications, Energy Procedia 49 (2014) 1187–1196, https://doi.org/10.1016/j.egypro.2014.03.128.

[15] C.M. Invernizzi, Prospects of mixtures as working fluids in real-gas Brayton cycles, Energies 10 (10) (2017), https://doi.org/10.3390/en10101649.

[16] M. Binotti, M. Astolfi, S. Campanari, G. Manzolini, P. Silva, Preliminary assessment of sCO2 cycles for power generation in CSP solar tower plants, Appl. Energy 204 (2017) 1007–1017, https://doi.org/10.1016/j.apenergy.2017.05.121.

[17] L. Wang, L. Pan, J. Wang, D. Chen, Y. Huang, L. Hu, Investigation on the temperature sensitivity of the S-CO2 Brayton cycle efficiency, Energy 178 (Jul. 2019) 739–750, https://doi.org/10.1016/j.energy.2019.04.100.

[18] S. Khatoon, M.H. Kim, Potential improvement and comparative assessment of supercritical Brayton cycles for arid climate, Energy Convers. Manag. 200 (September) (2019) 112082, https://doi.org/10.1016/j.enconman.2019.112082.

[19] J.I. Linares, M.J. Montes, A. Cantizano, C. Sánchez, A novel supercritical CO2 recompression Brayton power cycle for power tower concentrating solar plants, Appl. Energy 263 (October 2019) (2020) 114644, https://doi.org/10.1016/j.apenergy.2020.114644.

[20] M.M. Ehsan, Z. Guan, H. Gurgenci, A. Klimenko, Feasibility of dry cooling in supercritical CO2 power cycle in concentrated solar power application: Review and a case study, Renew. Sust. Energ. Rev. 132 (November 2019) (2020) 110055, https://doi.org/10.1016/j.rser.2020.110055.

[21] M. Saeed, M.H. Kim, Analysis of a recompression supercritical carbon dioxide power cycle with an integrated turbine design/optimization algorithm, Energy 165 (2018), https://doi.org/10.1016/j.energy.2018.09.058.

[22] K. Alawadhi, A. Alfalah, B. Bader, Y. Alhouli, A. Murad, An optimization study to evaluate the impact of the supercritical CO2 Brayton cycle's components on its overall performance, Appl. Sci. 11 (5) (2021), https://doi.org/10.3390/app11052389.

[23] A. Goyal, A.F. Sherwani, D. Tiwari, Optimization of cyclic parameters for ORC system using response surface methodology (RSM), Energy Sour. Part A Recover. Util. Environ. Eff. 43 (8) (2021) 993–1006, https://doi.org/10.1080/15567036.2019.1633443.

[24] C. Song, Y. Kitamura, S. Li, Optimization of a novel cryogenic CO2 capture process by response surface methodology (RSM), J. Taiwan Inst. Chem. Eng. 45 (4) (2014) 1666–1676, https://doi.org/10.1016/j.jtice.2013.12.009.

[25] F. Benayoun, D. Boumezerane, S.R. Bekkouche, F. Ismail, Optimization of geometric parameters of soil nailing using response surface methodology, Arab. J. Geosci. 14 (19) (2021), https://doi.org/10.1007/s12517-021-08280-z.

[26] S.R. Sundara Bharathi, D. Ravindran, A. Arul Marcel Moshi, R. Rajeshkumar, R. Palanikumar, Multi objective optimization of CNC turning process parameters with acrylonitrile butadiene styrene material, Mater. Today Proc. 27 (xxxx) (2019) 2042–2047, https://doi.org/10.1016/j.matpr.2019.09.055.

[27] J.I. Madsen, W. Shyy, R.T. Haftka, Response surface techniques for diffuser shape optimization, AIAA J. 38 (9) (2000) 1512–1518, https://doi.org/10.2514/2.1160.

[28] H. Sun, Wind turbine airfoil design using response surface method, J. Mech. Sci. Technol. 25 (5) (2011) 1335–1340, https://doi.org/10.1007/s12206-011-0310-6.

[29] M. Bertini, D. Fiaschi, G. Manfrida, P.H. Niknam, L. Talluri, Evaluation of the property methods for pure and mixture of CO2 for power cycles analysis, Energy Convers. Manag. 245 (Oct. 2021) 114568, https://doi.org/10.1016/j.enconman.2021.114568.

[30] X. Liu, Z. Xu, Y. Xie, H. Yang, CO2-based mixture working fluids used for the dry-cooling supercritical Brayton cycle: thermodynamic evaluation, Appl. Therm. Eng. 162 (17923) (Nov. 2019) 114226, https://doi.org/10.1016/j.applthermaleng.2019.114226.

[31] Aspen Plus | Leading Process Simulation Software | AspenTech. https://www.aspentech.com/en/products/engineering/aspen-plus.

[32] Z. Mohammadi, M. Fallah, S.M.S. Mahmoudi, Advanced exergy analysis of recompression supercritical CO2 cycle, Energy (2019), https://doi.org/10.1016/j.energy.2019.04.134.

[33] M. Martín, Optimal annual operation of the dry cooling system of a concentrated solar energy plant in the south of Spain, Energy 84 (2015) 774–782, https://doi.org/10.1016/j.energy.2015.03.041.

[34] R.N. Henson, Analysis of Variance (ANOVA) vol. 1, Elsevier Inc., 2015.

[35] T. Neises, Steady-state off-design modeling of the supercritical carbon dioxide recompression cycle for concentrating solar power applications with two-tank sensible-heat storage, Sol. Energy 212 (Dec. 2020) 19–33, https://doi.org/10.1016/j.solener.2020.10.041.

[36] R. Chen, M. Romero, J. González-Aguilar, F. Rovense, Z. Rao, S. Liao, Design and off-design performance comparison of supercritical carbon dioxide Brayton cycles for particle-based high temperature concentrating solar power plants, Energy Convers. Manag. 232 (October 2020) (2021), https://doi.org/10.1016/j.enconman.2021.113870.

[37] M.S. Salim, M. Saeed, M.H. Kim, Performance analysis of the supercritical carbon dioxide re-compression Brayton cycle, Appl. Sci. 10 (3) (2020), https://doi.org/10.3390/app10031129.

[38] M.A. Reyes-Belmonte, A. Sebastián, M. Romero, J. González-Aguilar, Optimization of a recompression supercritical carbon dioxide cycle for an innovative central receiver solar power plant, Energy 112 (2016) 17–27, https://doi.org/10.1016/j.energy.2016.06.013.

[39] M. Monjurul Ehsan, "Investigating the Effect of Dry Cooling System Design on the Performance of Supercritical CO2 Cycle in Concentrated Solar Power Application School of Mechanical and Mining Engineering".

[40] R. Dwornicka, J. Pietraszek, The outline of the expert system for the design of experiment, Prod. Eng. Arch. 20 (20) (2018) 43–48, https://doi.org/10.30657/pea.2018.20.09.

[41] E. Morosini, A. Ayub, G. di Marcoberardino, C.M. Invernizzi, P. Iora, G. Manzolini, Adoption of the CO2 + SO2 mixture as working fluid for transcritical cycles: a thermodynamic assessment with optimized equation of state, Energy Convers. Manag. 255 (Mar. 2022) 115263, https://doi.org/10.1016/j.enconman.2022.115263.

[42] G. Di Marcoberardino, E. Morosini, G. Manzolini, Preliminary investigation of the influence of equations of state on the performance of CO2 + C6F6 as innovative working fluid in transcritical cycles, Energy 238 (Jan. 2022) 121815, https://doi.org/10.1016/j.energy.2021.121815.

[43] F. Crespi, et al., Thermal efficiency gains enabled by using CO2 mixtures in supercritical power cycles, Energy 238 (Jan. 2022) 121899, https://doi.org/10.1016/j.energy.2021.121899.

[44] J. Sarkar, S. Bhattacharyya, Optimization of recompression S-CO2 power cycle with reheating, Energy Convers. Manag. 50 (8) (2009) 1939–1945, https://doi.org/10.1016/j.enconman.2009.04.015.

[45] J. Sarkar, Second law analysis of supercritical CO2 recompression Brayton cycle, Energy 34 (9) (2009) 1172–1178, https://doi.org/10.1016/j.energy.2009.04.030.